

Electromagnetic Environments and Wireless Channels for Through-the-Earth (TTE) Communications in an Underground Coal Mine: Modeling and Measurements

Chenming Zhou* and Nicholas Damiano

Abstract—Through-the-earth (TTE) communication systems are useful for post-disaster emergency communications due to their likelihood of surviving a mine disaster. The wireless channel and electromagnetic environment (EME) are two primary factors that affect the performance of a TTE system and have not been well understood in a mining environment. This paper reports our recent measurements conducted in an active coal mine to characterize the wireless channel and EME of a TTE system. TTE transmissions were successfully demonstrated in a mine location with a depth of 567 m (1,860 ft) by using ground rods installed on the surface and existing roof bolts in the underground. The results show that the EME in the mine is dominated by the 60-Hz signal and its harmonics for both surface and underground environments. The signal attenuation caused by the channel increases for frequencies greater than 90 Hz, which appears to be an optimum frequency point showing the smallest attenuation. An analytical path loss model for TTE channels is developed and validated using measurement results. This paper provides a measured data set as well as a model that an electric-field TTE system operator or system designer can reference when implementing TTE technologies in a mining environment.

1. INTRODUCTION

Through-the-earth (TTE) communications (sometimes also called sub-surface communications [1]) use extremely low frequency (ELF) or low-frequency (LF) waves to communicate directly through the earth overburden which is generally opaque to higher-frequency conventional radio signals [2–6]. TTE communication systems require less infrastructure that can be exposed to damage in the case of fire, explosion or large ground-fall. As a result, TTE systems are more likely to survive from a mining disaster during which conventional communication systems might be impaired.

A TTE system can be categorized as either a magnetic-field system or an electric-field (E-field) system, based on the fields that the system uses for communicating messages. A magnetic-field-based system typically uses a current loop at the transmitter side to generate strong magnetic fields and then another loop or ferrite coil to receive the fields [7]. An E-field TTE system, which is the focus of this paper, uses one set of electrodes to inject electric currents into the earth and another set of electrodes on the other end of the overburden to receive the E-field signals. Fig. 1 illustrates an E-field TTE system deployed in a mine where ground rods (shown as an inset) are used to inject current into the earth.

One of the major challenges for TTE communications is the severe signal attenuation caused by the earth overburden as signals travel through the earth overburden. This signal attenuation can be characterized by the path loss of the TTE channel. While the path loss of a wireless channel has been

Received 16 April 2021, Accepted 25 June 2021, Scheduled 6 July 2021

* Corresponding author: Chenming Zhou (czhou@cdc.gov).

The authors are with the Pittsburgh Mining Research Division, National Institute for Occupational Safety and Health, Pittsburgh, PA, USA.

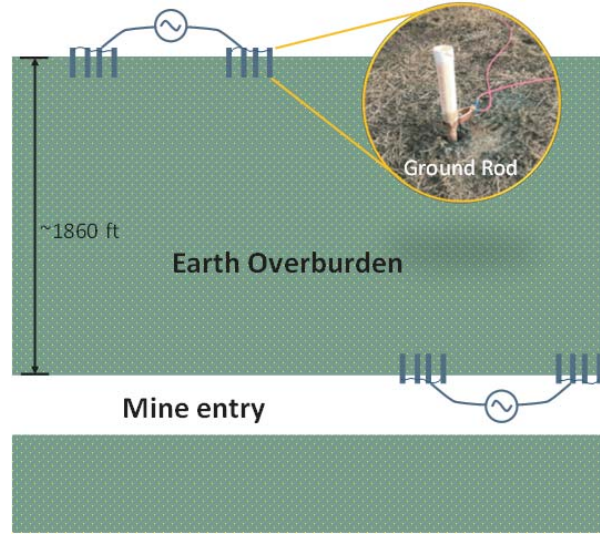


Figure 1. An electrode-based TTE communication system used in a coal mine. The inset shows an example of the installed ground rods on the surface.

well understood at conventional frequency bands, there has been limited research concerning a wireless TTE channel in the ELF and LF bands, particularly in an underground mining environment. In 2001, a frequency domain channel sounding method was employed to characterize the wireless channel for E-field TTE communications on the surface in a public park environment [8]. TTE channel characterization and system design were also discussed by Gibson in his Ph.D. dissertation [9].

In addition to the channel, the performance of a TTE system is also greatly impacted by the electromagnetic environments (EMEs) where the system is operated [10, 11]. Historically extensive electromagnetic noise surveys have been conducted in different mines by the U.S. Bureau of Mines in the 1970s [11–15]. Changes in the design and operation of electrical equipment used in mining since then have resulted in changes in the EME. Consequently, there is a need to evaluate the EME in a current representative mining environment to ensure that TTE systems will operate under emergency conditions when they are needed the most.

In this paper, we report our recent measurement results on characterizing the communication channel and EME for an electric-field-based TTE system in an active coal mine. We demonstrated that TTE signals can penetrate 567 m (1,860 ft) of earth overburden and still be detectable in the underground. Additionally, we developed an analytical model to approximate the path loss of a TTE channel and validated the model with measurement results.

It should be noted that, to our best knowledge, this paper is one of the few papers reporting TTE measurements in a relatively deep (depth > 1,000 ft) underground coal mine, as the depth of the mines reported in the literature is typically less than 1,000 ft [16].

The rest of the paper is organized as follows: Section 2 introduces the model for characterizing TTE channels. Section 3 describes the measurement system and set up for characterizing TTE channel and EME in an active coal mine, with the corresponding results being discussed in Section 4. Finally, Section 5 presents our conclusions.

2. MODELING WIRELESS CHANNELS FOR TTE COMMUNICATIONS

For TTE communications in mining applications, the separation distance between a transmitter and a receiver is generally much less than one wavelength. As a result, only the channel loss will be studied, and the phase associated with the channel is neglected. To study the channel loss, the voltage signal induced in the receiver antenna for a given transmitted power needs to be determined. This voltage signal at the receiver can be obtained by integrating the E-field over the length of the receiver antenna. Consequently, the problem of characterizing a TTE channel becomes the problem of solving

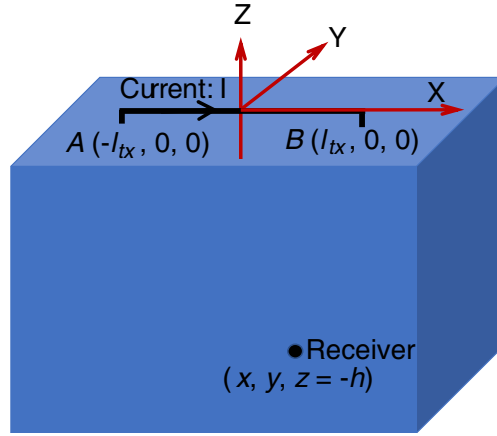


Figure 2. The transmitter antenna of a TTE system is modeled as a grounded line source on a homogeneous conducting half-space (i.e., the earth).

the subsurface fields of a finite line source.

As shown in Fig. 2, the transmitter antenna which is assumed to be a straight insulated current carrying cable can be modeled as a line source with a finite length of $2l_{tx}$. The two ends of the cable are grounded through electrodes to the earth which is assumed to be a homogeneous conducting half-space with a conductivity of σ . For mathematical convenience, the origin of the Cartesian coordinate is placed in the center of the cable with the x -axis being oriented along the same direction of the cable. Assuming that the cable carries a constant current I and lies directly above the ground (i.e., the distance between the cable and the ground is negligible), the E-field components of an underground observation point located at (x, y, z) caused by the line source have been solved by Hill and Wait [1], and are given by:

$$E_x = \frac{-I}{2\pi\sigma} \int_{-l_{tx}}^{l_{tx}} \left(\frac{\partial^2 P}{\partial z^2} + \frac{\partial^3 N}{\partial y^2 \partial z} \right) dx' \tag{1}$$

$$E_y = \frac{I}{2\pi\sigma} \int_{-l_{tx}}^{l_{tx}} \left(\frac{\partial^3 N}{\partial y \partial x \partial z} \right) dx' \tag{2}$$

$$E_z = \frac{I}{2\pi\sigma} \int_{-l_{tx}}^{l_{tx}} \left(\frac{\partial^2 P}{\partial x \partial z} \right) dx' \tag{3}$$

where $P = \frac{\exp(-\gamma R)}{R}$, $N = I_0[(\frac{\gamma}{2})(R+z)]K_0[(\frac{\gamma}{2})(R-z)]$, $R = \sqrt{y^2 + (x-x')^2 + z^2}$, $\gamma = \sqrt{i2\pi f\mu_0\sigma}$, I_0 and K_0 are modified Bessel functions of order zero. Here, μ_0 is the permeability of free space, and f is the system operating frequency. After some mathematical manipulations, partial derivatives of P and N in (1)–(3) can be expressed as:

$$\begin{aligned} \frac{\partial^2 P}{\partial z^2} &= \frac{e^{-\gamma R}}{R^2} \left[\frac{1}{R} \left(-1 + \frac{3z^2}{R^2} \right) + \gamma \left(-1 + \frac{3z^2}{R^2} \right) + \frac{\gamma^2 z^2}{R} \right] \\ \frac{\partial^3 N}{\partial y^2 \partial z} &= \frac{\gamma}{2} [B_{00}I_0K_0 + B_{11}I_1K_1 + B_{01}I_0K_1 + B_{10}I_1K_0] \\ \frac{\partial^3 N}{\partial x \partial y \partial z} &= \frac{\gamma}{2} [A_{00}I_0K_0 + A_{11}I_1K_1 + A_{01}I_0K_1 + A_{10}I_1K_0] \\ \frac{\partial^2 P}{\partial x \partial z} &= \frac{e^{-\gamma R}(x-x')z}{R^3} \left(\frac{3}{R^2} + \frac{3\gamma}{R} + \gamma^2 \right) \end{aligned}$$

where

$$B_{00} = \frac{\gamma z}{R} \left(1 - \frac{3y^2}{R^2} \right)$$

$$\begin{aligned}
B_{11} &= \frac{\gamma z}{R^2} \left(-1 + \frac{3y^2}{R^2} + \frac{2y^2}{y^2 + (x - x')^2} \right) \\
B_{01} &= \frac{1}{R^2} \left(-1 + \frac{z(1 - \gamma^2 y^2)}{R} + \frac{3y^2}{R^2} - \frac{3y^2 z}{R^3} \right) \\
B_{10} &= \frac{1}{R^2} \left(-1 - \frac{z(1 - \gamma^2 y^2)}{R} + \frac{3y^2}{R^2} + \frac{3y^2 z}{R^3} \right) \\
A_{00} &= \frac{-3(x - x') y z \gamma}{R^4} \\
A_{01} &= \frac{(x - x') y [3(R - z) - zR^2 \gamma^2]}{R^5} \\
A_{10} &= \frac{(x - x') y [3(z + R) + zR^2 \gamma^2]}{R^5} \\
A_{11} &= \frac{(x - x') y z \gamma (5R^2 - 3z^2)}{R^4 [R^2 - z^2]}
\end{aligned}$$

The received signal, i.e., the voltage in the receiver antenna, can be obtained by integrating the E-field over the length of the receiver antenna as:

$$V_{rx} = \int \vec{E} \cdot d\vec{l}_{rx} \quad (4)$$

For deep mines (i.e., z is large) where E-fields do not vary significantly over the length of the receiver antenna, Eq. (4) can be approximated as

$$V_{rx} \approx 2El_{rx} \cos \theta \quad (5)$$

where $2l_{rx}$ is the length of the receiver antenna, and θ is the angle between the E-field and the receiver antenna. The corresponding E-field strength then can be calculated by:

$$E = \sqrt{E_x^2 + E_y^2 + E_z^2} \quad (6)$$

Let $PL = 20 \log_{10}(|V_{tx}|/|V_{rx}|)$ denote the path loss of a TTE channel, where $V_{tx} = IZ_{tx}$ is the voltage signal at the transmitter antenna, substituting Eqs. (1)–(3) into Eq. (5) which leads to

$$PL(l_{tx}, l_{rx}, Z_{tx}, \theta, R, f, \sigma) \approx 20 \log_{10} \left[\frac{\pi \sigma |Z_{tx}|}{F(\sigma, R, f, l_{tx}) l_{rx} \cos \theta} \right] \quad (7)$$

where

$$F(\sigma, R, f, l_{tx}) = \sqrt{\left[\int_{-l_{tx}}^{l_{tx}} \left(\frac{\partial^2 P}{\partial z^2} + \frac{\partial^3 N}{\partial y^2 \partial z} \right) dx' \right]^2 + \left[\int_{-l_{tx}}^{l_{tx}} \left(\frac{\partial^3 N}{\partial y \partial x \partial z} \right) dx' \right]^2 + \left[\int_{-l_{tx}}^{l_{tx}} \left(\frac{\partial^2 P}{\partial x \partial z} \right) dx' \right]^2} \quad (8)$$

It can be found from Eq. (7) that the path loss of a TTE channel is determined by the following controlling factors:

- Tx and Rx antenna lengths (i.e., l_{tx} and l_{rx}).
- Conductivity (σ).
- Frequency (f).
- The orientation of the Rx antenna relative to the E-field (θ).
- Impedance between electrodes for TX ($|Z_{tx}|$).
- The location of Rx relative to Tx (R).

It should be noted that in this paper the frequency is assumed to be sufficiently low so that displacement currents can be neglected. This assumption is well justified for TTE communications where the length of the cable (i.e., the antenna length) and the communication range are typically much less than one wavelength.

3. MEASURING WIRELESS CHANNEL AND ELECTROMAGNETIC NOISE IN MINING ENVIRONMENTS

3.1. Experimental Setup

To characterize TTE communication channels and EMEs in a mining environment, four researchers from the National Institute for Occupational Safety and Health (NIOSH) made TTE measurements in an active coal mine located in the southern U.S. in November 2019. To prepare for the tests, two ground beds were installed on the surface in a relatively flat and open area covered by grass. As shown in Fig. 3, the two constructed ground beds were separated by 73.8 m (242 ft) with each consisting of an array of 24 four-foot-long copper-clad ground rods. Connections to each electrode were made using stranded 10-gauge copper wire. The inset in Fig. 1 shows an example of the ground rods installed on the surface. In the underground, no ground rods were installed. Instead, existing roof bolts were used to demonstrate that roof bolts may be used as the required electrodes for a TTE transmission. Fig. 4 shows pictures of the mine entry and an example of the roof bolts that were used in the underground. The separation distance between the two roof bolt arrays in the underground is about 12.1 m (40 ft). The overburden of the mine is about 567 m (1860 ft) and there is a horizontal offset of about 152.4 m (500 ft) between the surface ground beds and the underground TTE electrodes. It should be noted that



Figure 3. A satellite image depicting the approximate locations of the surface and underground electrodes.

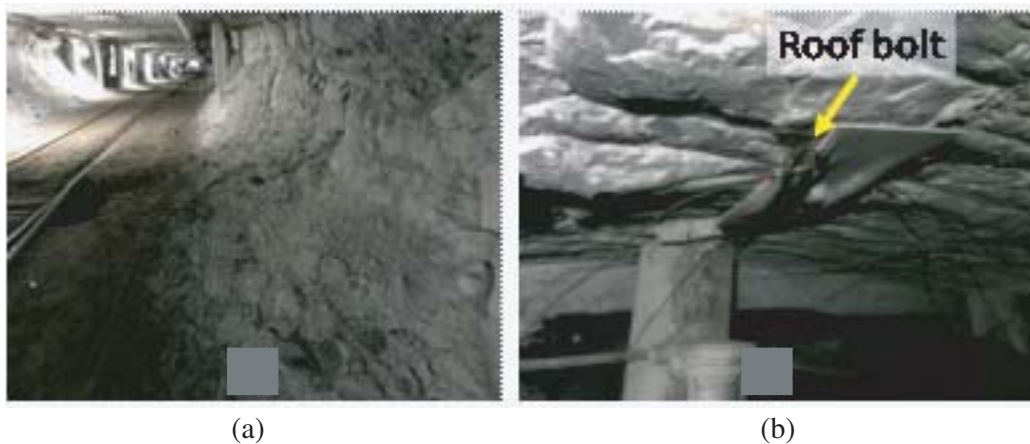


Figure 4. TTE measurements in an underground coal mine. (a) shows a picture of the mine entry in the underground, and (b) shows one of the roof bolts used as the electrode for TTE signaling.

accurately measuring the horizontal offset between the antenna on the surface and the antenna in the underground is not very practical, so the offset reported in the paper is based on our best estimation.

The transceiver used in the measurement (one on the surface and one in the underground) was a battery-powered prototype system developed by NIOSH. Transmitted signals were generated by a National Instruments Data Acquisition (NI-DAQ) module (NI-9269). An audio amplifier was used to boost the transmitted signal. To measure the transmitted current, a 0.1-ohm resistor was added into the wire connecting the amplifier and the ground bed. The voltage dropped over the 0.1-ohm resistor was recorded by the same NI-DAC which sampled at 50 k samples/sec. For the receiver, signals from the wire connected to electrodes were directly fed into one of the analog input ports of the NI-DAC. More details about the measurement system can be found in [16].

3.2. Experiment Description

First, to characterize the EME in a mining environment, background E-fields were recorded for both the underground and the surface without transmitting any signal. Second, to characterize the TTE channel, signals were transmitted across a frequency range of 30–2010 Hz at 34 discrete frequencies with a frequency spacing of 60 Hz. For each frequency, the signal was transmitted for 3 seconds followed by a 0.1-second gap. These frequencies were chosen to avoid the 60-Hz signal and its harmonics. A 330-Hz Continuous Wave (CW) pulse was transmitted immediately before and after each channel sounding for the purpose of synchronization. During the channel sounding process, transmitted currents were recorded at the transmitter and received voltages were recorded at the receiver.

4. RESULTS AND DISCUSSION

4.1. Measured Electromagnetic Environments

Figure 5 illustrates the power spectrum of the measured E-field noise on the surface, when there is no target signal transmitted from the underground. The power spectrum was obtained by dividing the measured time domain waveform into small segments and applying a Fourier transform to each segment. A windowing (Hanning window) function was applied to reduce spectrum leakage. In Fig. 5, the maximum and mean value of the power spectrum over different segments are labeled as “Max” and “Mean”, respectively. As expected, the strongest emission in the environment is the 60-Hz signal caused by the nearby power system. The harmonics of the 60-Hz signal were noticeable as well. There is about a 10-dB difference between the mean value and the max value of the noise floor. The difference between the max and mean value is less for frequency components (e.g., 60 Hz and its harmonics) with a higher power.

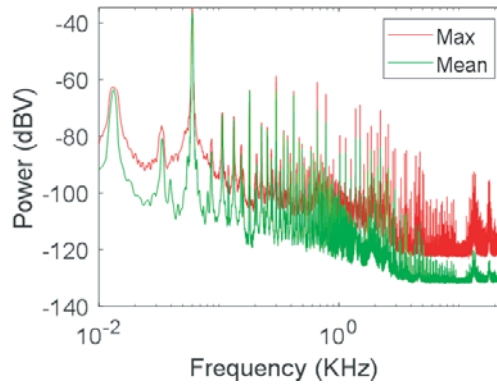


Figure 5. Measured EME on the surface when there is no signal transmitted from the underground.

Figure 6 shows a comparison of the measured power spectrum for the underground and the surface. To simplify the plots, only mean values are compared. It is interesting to note that emissions from the 60-Hz signal and its harmonics in the underground seem to be stronger than those measured on

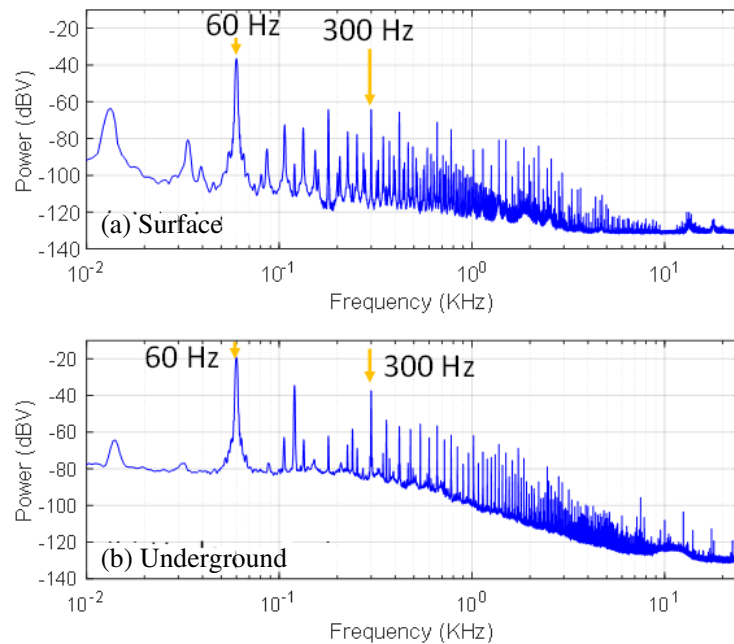


Figure 6. A comparison of the measured EME for different environments: (a) on the surface and (b) in the underground.

the surface. However, the electromagnetic energy measured on the surface appears to be distributed in more frequency components. For example, in Fig. 6, more “spikes” are observed between 60 Hz and 180 Hz on the surface than in the underground. For TTE communications, target signals should be chosen to avoid 60-Hz and its harmonics that exist in the environments.

4.2. Measured Channel Loss and Electromagnetic Interference

Figure 7 shows the spectrogram of the received signal in the underground as the transmitter on the surface swept across different frequency components. This spectrogram gives a visual representation of the spectrum of the received signal, as it varies with time. It is clear in Fig. 7 that target signals at frequencies from 30 Hz to 690 Hz transmitted from the surface can be visually identified from the

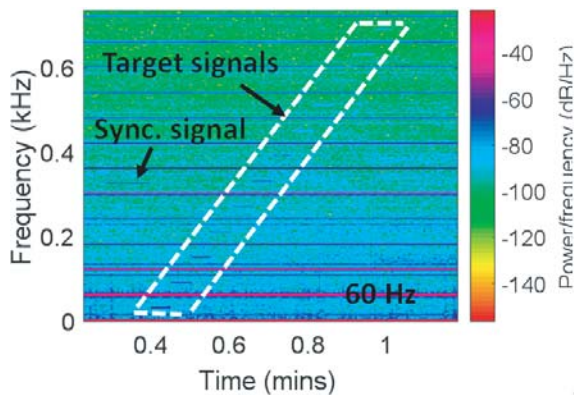


Figure 7. A spectrogram plot of the received signal in the underground with the presence of background EM noise.

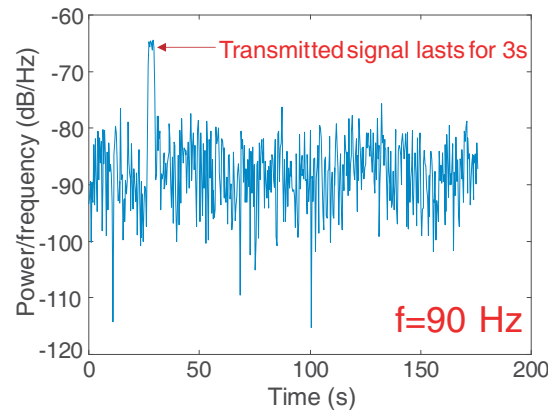


Figure 8. Received power variation over time at $f = 90$ Hz when the transmitter swept through different frequency components.

background noise (interference). The 60-Hz signal and its harmonics are also noticeable in Fig. 7. In contrast to target signals which were designed to last 3 seconds, the 60-Hz signal and its harmonics are continuous over time. The synchronization CW pulse at 330-Hz is also clear (as labeled) in Fig. 7.

To further quantify the received power for each frequency component, based on the results in Fig. 7, the variation of the received power over time for different frequencies can be plotted. Fig. 8 shows an example of such plots corresponding to the 90-Hz frequency component. It is clear in Fig. 8 that there is a power peak at around the -65 dB/Hz level which lasts about 3 seconds. The duration of this peak matches the duration of the transmitted CW pulse so this power peak can be reasonably attributed to the 3 s transmitted CW pulse at 90-Hz on the surface. As a result, the received power corresponding to the 90-Hz frequency component can be obtained by averaging the peak power in Fig. 8 over a time window of 3 seconds. Meanwhile, the interference power at 90-Hz can be obtained by computing the maximum or mean values of the received power over the full time window, excluding the 3-s time window in which the transmitter was transmitting a 90-Hz target signal.

Figure 9 shows the calculated received signal power for different target frequencies, normalized to the associated transmitted current at each frequency. Similarly, the calculated interference power for each frequency is also plotted for reference. The difference between the signal and the interference power can be viewed as signal-to-interference ratio (SIR), which is a key factor in determining the quality of wireless communications. It is shown in Fig. 9 that the channel loss at the tested location ranges from -102 dB/Hz to -65 dB/Hz, depending on the frequency. Generally, the channel introduces more attenuation to higher frequency signals. It is interesting to note that there appears to be an optimum frequency around 90 Hz which shows the minimum attenuation caused by the channel. This finding is consistent with the finding reported in [16] that was based on the measurement results from a different coal mine. Similar to the received signal power, the interference power also decreases with frequency. As a result, selecting low frequencies does not necessarily guarantee higher SIR as the value of SIR depends on both signal power and interference power in the environment at the selected frequencies.

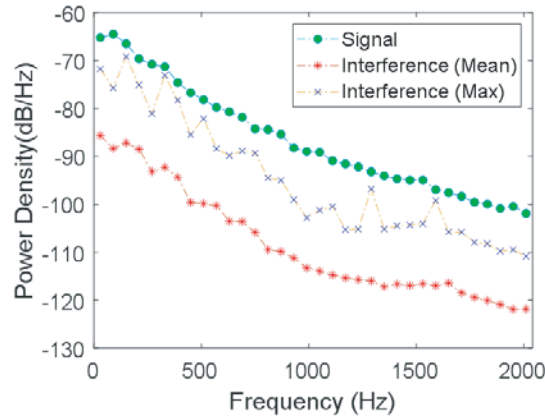


Figure 9. Signal (normalized to the transmitter current) and interference power received in the underground for different frequencies.

4.3. Simulated Received Power Distribution

Figure 10 is a heatmap to illustrate the distribution of E-field on the XZ plane directly underneath the transmitter antenna (i.e., for $y = 0$). The color at each location in Fig. 10 represents the strength of the E-field at that location, with yellow and blue representing the strongest and weakest fields, respectively. The associated contour plot where each point on a contour line has the same E-field is also given on the right. The E-field at each location on the XZ plane was computed based on (5). Key parameters used in the simulation, including the length of the transmitter and receiver antennas, overburden depth, and offset distance, were selected fully based on the actual parameters used in the measurements. The only exception is the average conductivity of the mine which is a parameter “created” in the simulation

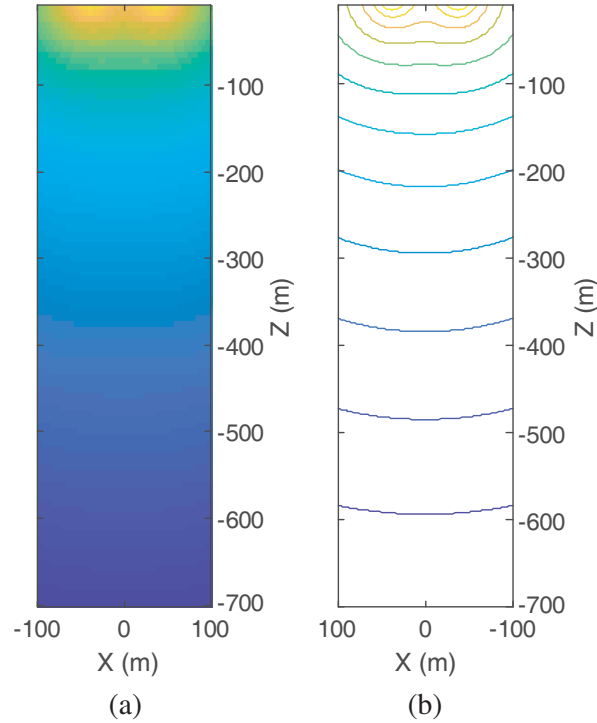


Figure 10. (a) Simulated E-field distribution on the XZ plane and (b) the associated contour plot.

that cannot be accurately and practically measured. It can be seen from Fig. 10 that the two grounded electrodes generate a strong E-field around them, and the E-field attenuates as the depth of the mine increases. The contour lines help visualize the shape of the E-field generated by the antenna. Similar to magnetic fields generated by a ferrite-rod antenna used in proximity detection systems, the E-field generated by a TTE linear antenna shows a peanut-like shape in areas close to the antenna and then gradually transitions to a water melon shape in areas deeper into the underground.

Similarly, Fig. 11 illustrates a simulated E-field distribution on the XY plane (i.e., the horizontal plane) for $z = -1860$ feet. This plot helps visualize the power variation that one can expect as a receiver antenna moves around horizontally inside the mine. It is clear in Fig. 11 that locations right underneath the transmitter (e.g., for $x = 0$ and $y = 0$) has the maximum E-field. It is also interesting to note that,

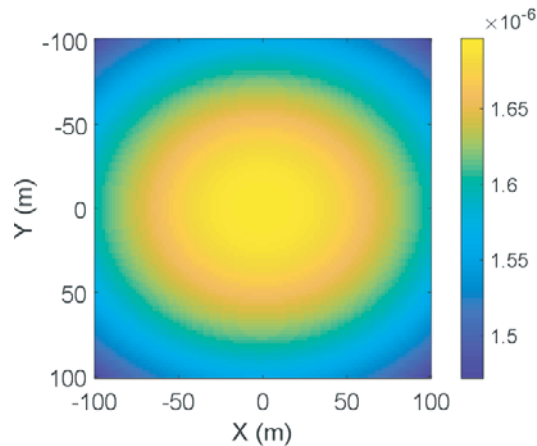


Figure 11. Simulated E-field distribution on the XY plane (horizontal plane in the mine) at $z = -1860$ feet.

based on the color bar shown in Fig. 11, the variation of the E-field in the XY plane is not significant, since the E-field variation over an area of $200 \times 200 \text{ m}^2$ is less than 10%. This finding confirms that the assumption made in Section 2 for the approximation in Eq. (5) is valid.

4.4. Model Validation

Figure 12 shows a comparison between the simulated and measured received power for different frequency components. Again, the simulation result was computed based on the actual parameters used in the measurements, except for the conductivity of the earth which has been used as a tuning parameter to best match the simulation results to the measurement results. It is found that by using a conductivity of 0.03 S/m , the simulation result shows a good agreement with the measurement results in terms of the turning point (i.e., at $f = 90 \text{ Hz}$) as well as the attenuation slope of the curve. It should be noted that in reality the conductivity value of the earth typically varies with different mines. The conductivity value (0.03 S/m) used in the simulation results reported in this paper is very close to the averaged measured conductivity value of 0.01 S/m reported in [17]. It is interesting to note that in Fig. 12 there appears to be a constant offset ($\sim 20 \text{ dB}$) between the simulated results and the measurement results. This offset suggests that an additional conversion factor may be needed to directly compare the absolute value of the simulated received power to the corresponding actual received power at a given frequency.

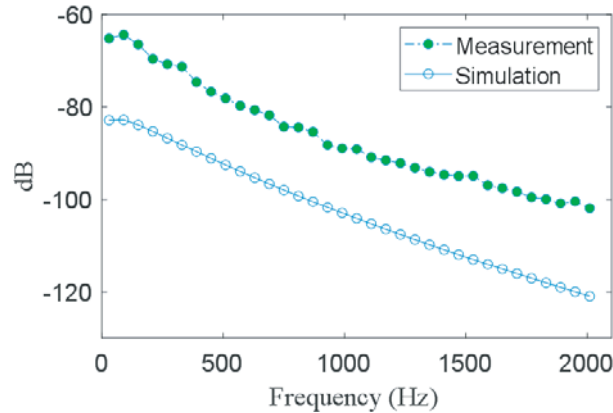


Figure 12. A comparison between simulated and measured received power for different frequency components.

5. CONCLUSION

In this study, TTE measurements were conducted in a deep active coal mine with an overburden depth of 1,860 ft using a customized channel sounding prototype system. The measurement results show that the channel loss generally increases for frequencies greater than 90 Hz which corresponds to the lowest path loss. A path loss model that can be implemented through the Matlab program was developed to predict the signal attenuation caused by a TTE channel. Simulated results based on the developed model also show an optimum frequency around 90 Hz and a similar power attenuation slope. In addition, the measured EMEs for both the surface and the underground environments were presented. It is found that the EME in the mine is dominated by the 60-Hz signal and its harmonics from the nearby power system. The results and findings in this paper can help better design and operate an E-field TTE system in a modern mining environment.

ACKNOWLEDGMENT

The authors would like to thank Cory DeGennaro, Justin Srednicki, and Lincan Yan for their help in collecting the measurement data.

DISCLAIMER

The findings and conclusions in this report are those of the authors and do not necessarily represent the official position of the National Institute for Occupational Safety and Health, Centers for Disease Control and Prevention. Mention of any company or product does not constitute endorsement by NIOSH.

REFERENCES

1. Hill, D. A. and J. R. Wait, "Subsurface electromagnetic fields of a grounded cable of finite length," *Canadian Journal of Physics*, Vol. 51, 1534–1540, 1973.
2. Zhou, C. and N. Damiano, "Wireless channels and electromagnetic environments for through-the-earth communications in a coal mine," *IEEE Radio Wireless Week*, 158–160, San Diego, CA, 2021.
3. Bae, S., Y.-K. Hong, J. Lee, J. Park, J. Jalli, G. S. Abo, H. M. Kwon, and C. K. Jayasooriya, "Pulsed ferrite magnetic field generator for through-the-earth communication systems for disaster situation in mines," *Journal of Magnetism*, Vol. 18, No. 1, 43–49, 2013.
4. Geyer, R. G. and G. V. Keller, "Constraints affecting through-the-earth electromagnetic signalling and location techniques," *Radio Science*, Vol. 11, No. 4, 323–342, 1976.
5. J. Carreño, L. Silva, S. Neves, L. Aguayo, A. J. Braga, A. N. Barreto, and L. U. Garcia, "Through-the-earth (TTE) communications for underground mines," *Journal of Communication and Information Systems*, Vol. 31, No. 1, 2016.
6. Yenchek, M. R., G. T. Homce, N. W. Damiano, and J. R. Srednicki, "NIOSH-sponsored research in through-the-earth communications for mines: A status report," *IEEE Transactions on Industry Applications*, Vol. 48, No. 5, 1700–1707, 2012.
7. Wait, J. and K. Spies, "Subsurface electromagnetic fields of a circular loop of current located above ground," *IEEE Transactions on Antennas and Propagation*, Vol. 20, No. 4, 520–522, 1972.
8. Bataller, V., A. Munoz, N. Ayuso, and J. Villarroel, "Channel estimation in through-the-earth communications with electrodes," *Progress In Electromagnetics Research*, Vol. 7, No. 5, 486–490, 2001.
9. Gibson, D., "Channel characterisation and system design for sub-surface communications," Ph.D. thesis, University of Leeds, 2010.
10. Muñoz, A., V. Bataller, N. Ayuso, P. Molina, A. Mediano, J. Cuchi, and J. Villarroel, "Noise characterization in through-the-earth communications with electrodes," *Progress In Electromagnetics Research Symposium Abstracts*, 1521, Marrakesh, Morocco, March 20–23, 2011.
11. Adams, J. W., "Summary report on electromagnetic noise measurement program," Contract Final Report submitted to the United States Bureau of Mines, 1973.
12. Adams, J. W., W. Bensema, and M. Kanda, "Electromagnetic noise in grace mine," Final report prepared for U.S Bureau of Mines, 1974.
13. Scott, W., J. Adams, W. Bensema, and H. Dobroski, "Electromagnetic noise in Lucky Friday mine," Contract Final Report submitted to the United States Bureau of Mines, 1974.
14. Kanda, M., J. W. Adams, and W. Bensema, "Electromagnetic noise in McElroy mine," Contract Final Report submitted to the United States Bureau of Mines, 1974.
15. Bensema, W., M. Kanda, and J. W. Adams, "Electromagnetic noise in Itmann mine."
16. Yan, L., C. Zhou, M. Reyes, B. Whisner, and N. Damiano, "Mathematical modeling and measurement of electric fields of electrode-based through-the-earth (TTE) communication," *Radio Science*, Vol. 52, No. 6, 731–742, 2017.
17. Geyer, R., G. Keller, and T. Ohya, "Research on the transmission of electromagnetic signals between mine workings and the surface," Contract report submitted to the United States Bureau of Mines, 1974.